World Scientific
www.worldscientific.com

OPTICAL COHERENCE TOMOGRAPHY FOR BLADDER CANCER DIAGNOSIS: FROM ANIMAL STUDY TO CLINICAL DIAGNOSIS

ZHIJIA YUAN*, HUGANG REN*, WAYNE WALTZER†, JASON KIM†,
JINGXUAN LIU**, KEMIAO JIA‡, HUIKAI XIE‡ and YINGTIAN PAN*,§

Departments of Biomedical Engineering, Urology†, and Pathology**
Stony Brook University, Stony Brook, NY, USA*

‡The ECE Department, University of Florida,
Gainesville, FL, USA
§yingtian.pan@sunysb.edu

This paper summarizes the recent technological development in our lab on cystoscopic optical coherence tomography (COCT) by integrating time-domain OCT (TDOCT) and spectral-domain OCT (SDOCT) with advanced MEMS-mirror technology for endoscopic laser scanning imaging. The COCT catheter can be integrated into the instrument channel of a commercial 22Fr rigid cystoscopic sheath for in vivo imaging of human bladder under the cystosocopic visual guidance; the axial/transverse resolutions of the COCT catheter are roughly $9\,\mu m$ and $12\,\mu m$, respectively, and 2D COCT imaging can be performed with over 110dB dynamic range at 4–8 fps. To examine the utility and potential limitations of OCT for bladder cancer diagnosis, systemic ex vivo rat bladder carcinogenesis studies were performed to follow various morphological changes induced by tumor growth and in vivo porcine study was performed to examine the feasibility of COCT for in vivo imaging. Justified by promising results of the animal studies, preliminary clinical study was conducted on patients scheduled for operating-room cystoscopy for bladder cancers. Double-blind clinical results reveal that COCT can delineate detailed bladder architectures (e.g., urothelium, lamina propria, muscularis) at high resolution and detect bladder cancers based on enhanced urothelial heterogeneity as a result of excessive growing nature of bladder cancers. The diagnostic sensitivity and specificity can be enhanced to 92% and 85%, respectively. Results also suggest that due to reduced imaging depth of COCT in cancerous lesions, staging of bladder cancers may be limited to Ta or T1 for non-outgrowing cancerous lesions.

Keywords: Optical coherence tomography; bladder cancer diagnosis; microelectro-mechanical system.

1. Introduction

Bladder cancer is among the most common types of malignancies and the leading causes of death in the United States.[1] Clinical statistics reveal that most bladder cancers are superficial carcinomas that originate within the thin basal cell

§Corresponding author.

layers (20–200 μm) of the bladder epithelium or urothelium. Urothelial carcinomas (i.e., transitional cell carcinomas or TCCs) are curable if detected early (e.g., prior to invasion to the underlying muscularis) and treated appropriately; therefore, early diagnosis of TCC is of great clinical significance to the therapeutic benefits of bladder cancer patients. This, however, remains a clinical challenge. For instance, clinical screening techniques such as urine tests (including urine cytology and analysis, FISH, and BTA) are unable to provide sufficient sensitivity for low-grade, early bladder cancers. Current medical imaging modalities such as ultrasound, x-ray, computed tomography, and magnetic resonance imaging fail to detect early-stage TCCs due to limited spatial resolution and technical imperfections of these techniques. White-light cystoscopy by endoscopic visual inspection of bladder lesions is the current clinical standard for bladder cancer diagnosis. Cystoscopy can effectively diagnose papillary TCCs; however, it often misses flat bladder cancers such as carcinomas in situ that do not show distinctive outgrowth and relies on random biopsy, resulting in an overall low diagnostic sensitivity ($\sim 50\%$ for flat TCCs).[2,3] Therefore, a noninvasive and high-resolution imaging methodology is highly desirable to enhance current cystoscopic procedures in the detection of bladder cancers (e.g., non-papillary TCCs, tumor residuals) and staging of tumor invasions, and to guide the resection of bladder tumors.

In recent years, several optical imaging techniques have been developed to demonstrate the potential for noninvasive or minimally invasive detection of early bladder cancers. For instance, optical coherence tomography (OCT) is a promising technique that enables cross-sectional imaging at sub-10 μm axial resolution and 2–3 mm imaging depth,[4] thus offering great potential to delineate bladder architectures and the morphological changes (e.g., carcinogenesis) in the bladder epithelium and the underlying layers. Since the introduction of OCT to high-resolution imaging of the eye in early 90's, technological advances have dramatically improved the performances of the OCT systems: frequency-domain OCT greatly enhances the imaging rate of OCT to permit 2D and even 3D imaging of biological tissues *in vivo*,[5–7] Doppler OCT enables subsurface flow measurement and thus functional imaging,[8,9] polarization and spectroscopic OCT enhances the image contrast and sensitivity of OCT,[10–12] and ultrahigh-resolution OCT (e.g., $< 2\,\mu$m axial resolution) demonstrates the potential of subcellular imaging and thus more accurate diagnosis of early cancers (i.e., optical biopsy).[13–16] Endoscopic OCT, by combining fiber optically–based OCT with various advanced micro laser scanning techniques, allows miniature optical probes or catheters for noninvasive or minimally invasive *in vivo* OCT imaging of internal organs and thus diseases in these tissues.[17] In addition to technological advances, OCT has been applied to a wide variety of biological tissues such as skin,[18] oral cavity,[19] esophagus,[20] colon,[21] lung,[22] bladder,[23–25] cervix,[26] and intravascular vessels,[27] and results based on animal and human studies demonstrate the potential of OCT for high-resolution imaging diagnosis of various superficial cancers. Inspired by the initial success of OCT for high-resolution delineation of human bladder *ex vivo*, we have focused our research on OCT for bladder

cancer diagnosis since 1998. Here, we will summarize our work on the technological development of OCT suitable for bladder imaging both *ex vivo* and *in vivo*, which includes time-domain and spectral-domain OCT steroscopes for benchtop studies and MEMS-based cystoscopic OCT (COCT) and 5ALA-fluorescence guided COCT for *in vivo* studies. We will also summarize the results from *ex vivo* systemic animal carcinogenesis studies to *in vivo* animal and clinical diagnosis, which clearly demonstrates the potential of COCT to significantly enhance current cystoscopic procedures in the diagnosis and treatment of early bladder cancers.

2. Technological Development

2.1. *Time-domain OCT (TDOCT) and spectral-domain OCT (SDOCT)*

Like most turbid biological tissues, urinary bladder not only absorbs and but also scatters light in the visible and NIR range. Light scattering degrades image contrast and reduces spatial resolution; therefore, advanced optical imaging methods such as OCT are required to reject multiple scattering and thus reconstruct the image. OCT operates analogously to ultrasound B-mode imaging in which ultrasound measures the time-gated echoes of a acoustic pulse whereas OCT detects coherence-gated backscattering of light from within the biological tissue. The core technology of OCT is low-coherence reflectometry for optical ranging; thereby, the axial resolution of OCT is defined by the coherence length,[28]

$$L_c = (2\ln 2/\pi) \cdot (\lambda^2/\Delta\lambda) \tag{1}$$

where λ, $\Delta\lambda$ are the central wavelength and the full-width-half-maximum (FWHM) spectral bandwidth of the broadband source (BBS). Implementation of OCT imaging can be in either time domain (TDOCT) or spectral domain (SDOCT).[29] Since both methods have been reported previously, only a brief introduction to the principles of these two methods will be provided here. Figures 1(A) and (B) illustrates the principles of TDOCT and SDOCT. A fiber optic Michelson interferometer is illuminated by a pigtailed broadband light source with output power of $12\,\mathrm{mW}$, central wavelength at $1310\,\mathrm{nm}$ and FWHM spectral bandwidth of $78\,\mathrm{nm}$ (yielding a coherence length of $L_c \approx 10\,\mu\mathrm{m}$). The input light is equally divided into the two arms of the Michelson interferometer ($50\%:50\%$). For TDOCT (a), the light from in the reference arm is collimated to $\phi 2.4\,\mathrm{mm}$ by an angle-polished GRIN lens (CM) and then guided to a rapid-scanning optical delay (RSOD)[30] for high-speed depth scanning (up to $2.4\,\mathrm{kHz}$ A-scan rate). A fiber-optic acousto-optic phase modulator (AOM) is used to provide accurate Doppler frequency f_D for optical heterodyne detection, which is implemented by nulling the phase shift induced in the RSOD (i.e., centering the scanning mirror) and inserting a pair of differential AOMs (i.e., one upshifted at $55\,\mathrm{MHz}$ and one downshifted at $54\,\mathrm{MHz}$) to provide a ultra stable Doppler ($f_D = 2\,\mathrm{MHz} \pm 0.05\%$) signal for high-performance envelop detection.[31] This AOM-mediated RSOD ($f_D = 2\,\mathrm{MHz}$, $d^{-1} = 1200/\mathrm{mm}$, $f = 80\,\mathrm{mm}$) allows for
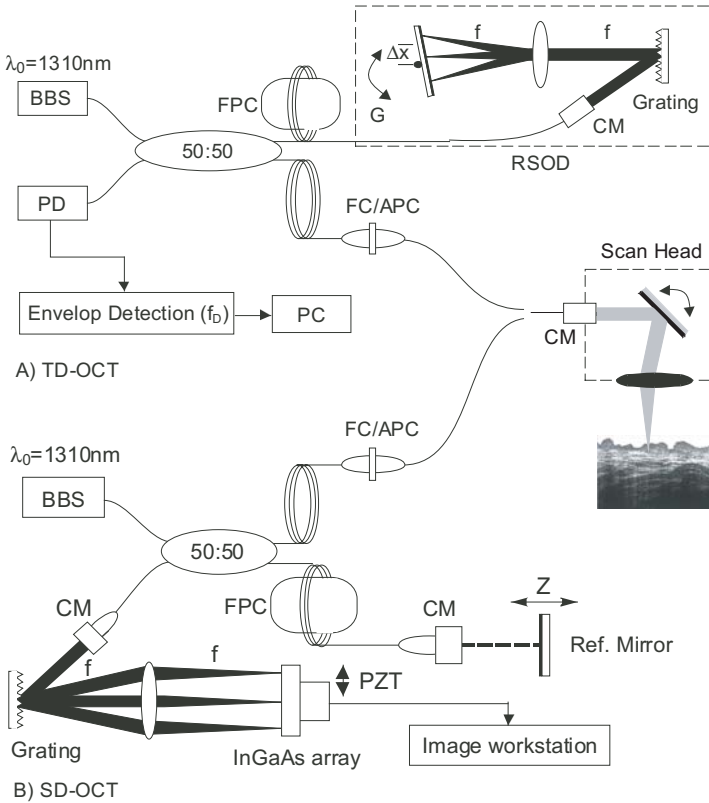
Fig. 1.   Schematic diagrams of TDOCT and SDOCT setups. (A) TD-OCT, (B) SD-OCT. BBS: broad band source, CM: collimator, FPC: fiber polarization controller, G: galvanometer Scanner, PD: photo diode, RSOD: rapid scanning optical delay line.

2.8 mm or higher axial scan with high system dynamic range (e.g., SNR >100 dB) at up to 2.4 kHz (limited by servo mirror), sufficient for the speed requirements of *in vivo* 2D bladder OCT (∼5 fps). The sample arm of the fiberoptic interferometer is connected to a handheld OCT stereoscope in which light is collimated to $\phi 5$ mm by a fiberoptic achromatic lens, scanned laterally by a $\phi 8$ mm servo mirror, and focused onto biological tissue under examination by a f/40 mm achromatic lens to yield a focal spot size (lateral resolution) of $\Delta r \approx 12\,\mu$m. The lateral scanning range which determines the field of view (FOV) in the transverse direction is approximately 6 mm. Then, the light beams from both sample and reference arms are recombined in the detection fiber and the detected interferometric signal is bandpass filtered at $f_D = 2$ MHz, amplitude linearly demodulated, and digitized via a 5 MHz, 12bit A/D for 2D for 2D and 3D OCT image reconstruction and display in either 12bit grayscale or pseudo color on a PC monitor at up to approximately 5 fps.

In contrast to TDOCT, mechanical scanning of the reference mirror to facilitate pathlength scan is circumvented, which is the major advantage of SDOCT

for high-speed OCT imaging. As shown in Fig. 1(B), light in the reference arm is collimated to $\phi 2$ mm by an angle-polished GRIN lens (CM) and then retroreflected by a stationary reference mirror which is placed on a motored stage to match the optical pathlengths between the sample and the reference arms of the fiberoptic interferometer. The light beams from the sample and reference arms are recombined in the detection fiber and then connected to a spectral radar imager in which light is collimated by a fiberoptic achromatic lens (f = 55 mm), and the spectral components are linearly projected by a diffraction grating ($d^{-1} = 1200$/mm) onto a fast line InGaAs photodiode array (Sensors Unlimited, NJ) placed on the focal plane of an achromatic lens system (f = 120 mm). The detected spectral profile containing spectrally encoded interference fringes from different depth within the bladder tissue is digitized via a 2-channel, 12-bit A/D at 5 MHz and processed by an image workstation, permitting full-size 2D OCT imaging at nearly 8 fps. Complex and computation-intensive data processing (e.g., spline interpolation for k = $2\pi/\lambda$ rescaling, inverse FFT) is required to convert spectral graph to an A-scan in an OCT image, but the use of powerful workstation and improved FFT computation has permitted instantaneous 2D OCT image display. For the parameters used in our current SDOCT, the axial resolution is $L_c \approx 9 \, \mu$m (approaching the theoretical limit) and the system dynamic range is enhanced to SNR ≈ 112 dB. However, the SNR degradation along the depth due to limited spectral resolution compromises the effective field of view of SDOCT in the axial direction and may induce artifacts (e.g., decay of OCT image contrast) to complicate clinical diagnosis. To tackle this problem, we proposed interpixel shifted SDOCT to restore the imaging depth, which was implemented by simply stepping the line InGaAs camera at a half interpixel shift (i.e., 12.5 μm) of the pixel size (25 μm) in the lateral direction to increase the pixel or spectral resolution of the spectral radar imager.[32] This simple method has proved effectively eliminating spectral aliasing artifact, restoring the useful imaging depth to 2.8 mm, and enhancing the SNR (13.6 dB) in deeper region (e.g., Δz > 1.5 mm), which can be critical to the staging of papillary TCC.

2.2. *MEMS-based cystoscopic OCT*

As a fiberoptic interferometric imaging technique, OCT can be integrated into a catheter endoscope for *in vivo* imaging of internal organs. Since the axial scan is implemented in the reference arm in TDOCT or spectral radar in SDOCT, transverse scan in the endoscope is required for 2D and even 3D OCT imaging, which remains a technical challenge. Bladder is large and flat; therefore, a front-view OCT catheter with surface imaging guidance is more suitable for clinical diagnosis. To tackle the challenge, we invented MEMS-based endoscopic OCT by employing microelectromechanical system (MEMS) mirror technology for high-fidelity endoscopic laser scanning,[33] taking advantage of the exceptional laser steering capability of MEMS mirror (high speed, precision, and coupling efficiency).[32,34,35] However, unlike those used for optical switch and display, the MEMS mirrors used

for endoscopic laser scanning require unique characteristics such as large actuation and mirror size, and high speed and linearity. Both electrothermal and electrostatic MEMS mirrors have been developed and tested for COCT. Based on our experimental results, typical mechanical actuation angle of $\theta_M(0v) \approx 17°$ is required to provide a lateral optical scanning range over $\theta = 2\theta_M \approx 35°$ for COCT imaging, and mirror size of $1.1 \times 1.2\,\text{mm}^2$ or larger is needed to suffice the NA (e.g., > 0.07) to ensure the image sensitivity and resolution required for delineating bladder morphology and diagnosing bladder cancers.[36]

Figure 2 shows the MEMS-based endoscopic OCT system. The sample arm of the fiberoptic SDOCT (A) is connected to a pigtailed OCT catheter through a modified FC/APC connector (panels B, C). The OCT catheter is inserted into instrument channel ($\phi 4\,\text{mm}$) of a 22Fr rigid endoscope sheath. A schematic of the optical arrangement in the distal OCT scope and a photograph of an OCT catheter are shown in panels (B) and (D). The light from the fiber is collimated by a 0.23-pitch selfoc lens to $\phi 1.1\,\text{mm}$, deflected by a pair of mirrors and then focused by a laser doublet ($f/10\,\text{mm}$) to a roughly $\phi 12\,\mu\text{m}$ spot size on the image plan. The transverse laser scan in the OCT catheter is facilitated by an Al-coated CMOS-MEMS planar mirror whose structure is shown by a scanning electron micrograph (SEM) in panel (E). This large $1.1 \times 1.2\,\text{mm}^2$ electrothermal mirror, fabricated by using DRIE CMOS-MEMS process, ensures large actuation range ($\theta_M \approx 17°$) and optical grade flatness ($\lambda/3$). The total laser steering range is $\theta = \pm 15°$ with applied electrical voltage under $10\,\text{V}$, fully complied with the medical safety requirement. Average imaging duration for COCT diagnosis is $< 10\,\text{min}$ per case. Examples
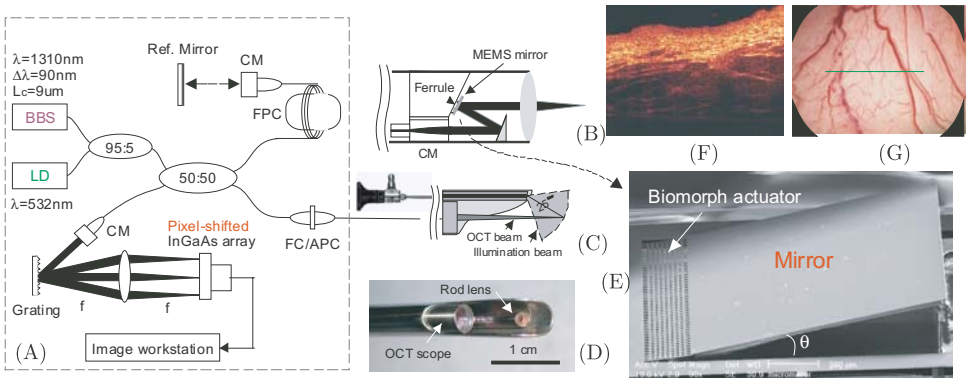

Fig. 2.   Sketch of MEMS-based COCT. (A) A sketch illustrating the SDOCT setup based on spectral radar as outlined in Fig. 1(B). A pixel-shifted InGaAs array is used for spectral OCT imaging. 2D OCT can be performed and displayed at 8–30 fps; (B, D) A $\phi 5\,\text{mm}$ COCT catheter; (C) White-light or fluorescence guidance; (E) A SEM graph of the $1.1 \times 1.2\,\text{mm}^2$ CMOS-MEMS mirror used in (B, D) for endoscopic laser scanning; and (F, G) Cross-sectional COCT and surface images of human bladder *in vivo*. BBS: broadband light source; FPC: fiber polarization controller; FC/APC: snap-on angled fiber connector; CM; Fiberoptic collimator; LD: 532 nm aiming green laser; f: focal length f = 132 mm; Rod lens: $25° \phi 2.7\,\text{mm}$ histoscope. COCT resolutions (lateral/transverse): $9\,\mu\text{m}/12\,\mu\text{m}$; FOV: $4.8 \times 2.4\,\text{mm}^2$.

of surface image and 2D cross-sectional COCT image of human bladder in vivo are given in Panels (F) and (G), respectively. Although our MEMS-based COCT can be performed under white-light surface imaging guidance, the FOV per COCT scan is less than 5 mm laterally regardless of its near real time image rate (e.g., 5–8 fps). One the other hand, white-light surface imaging may not effectively locate some unspecific bladder lesions (e.g., CIS) and thus results in enormous time for elaborate random scan of the entire bladder wall. To provide more effective surface imaging guidance for COCT scans, we proposed fluorescence image guided COCT by taking advantage of the high sensitivity of high 5ALA induced PpIX fluorescence in bladder tumors for rapid and effective diagnosis.[37] This can be implemented by simply modifying current white light imaging system with proper fluorescence filters (e.g., blue excitation at around 400 nm, emission at above 580 nm) to enhance fluorescence image contrast. Our animal studies have showed promising results for early bladder diagnosis with 100% sensitivity and 93% specificity (OCT drastically enhances the low specificity of fluorescence cystoscopy).[38] However, this technique has not been adopted in our clinical study for the following reasons: (1) 5ALA fluorescence cystoscopy has not been clinically approved in the US yet; (2) High cost associated with 5ALA and the 4.5 hr fluorescence induction (instillation); (3) White-light imaging guidance is sufficient for most OR cases we have encountered so far, so that all the COCT diagnoses can be completed in less than 10 minutes.

3. From Animal Study to Clinical Diagnosis

As a new biomedical imaging modality, OCT identification must be validated by established clinical techniques. OCT delineates bladder layers based on backscattering resulted from local refractive-index variations, whereas histology identifies bladder tissue compositions based on chemical dye (H&E) deposition on tissue slice. Thus, correlation of OCT with histology (gold standard for clinical diagnosis) is critical to confirm OCT identifications prior to clinical diagnosis. Summarized below are some of the results based on our *ex vivo* human specimen and animal carcinogenesis and *in vivo* clinical studies. Figure 3 shows a comparison between OCT and histology of human bladder specimen (fresh, unfrozen) *ex vivo*. The architectural
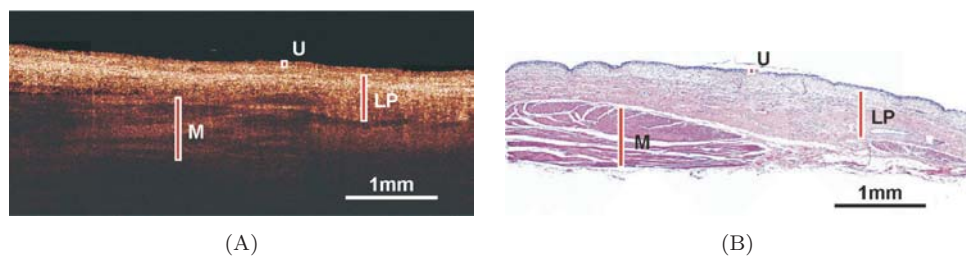

(A)   (B)

Fig. 3. Human bladder under proper stretch imaged by ex vivo OCT and histology, showing close correlations. Three important layers in the human bladder wall critical for the diagnosis of bladder cancer prognosis, e.g., urothelium (U), lamina propria (LP), and the upper muscularis (M) are delineated based on their backscattering differences.

layers of bladder wall from urothelium to upper muscularis correlate well between these two image modalities, e.g., the urothelium (U) of a normal bladder appears a uniform, thin, and low-scattering layer ($\sim 110\,\mu$m), and the lamina propria (LP) as a heterogeneous (e.g., blood vessels) and high scattering layer ($\sim 550\,\mu$m, may vary from place to place), The upper muscularis (M) appears largely bifurcated, representing the interfaces between the collagen bundles of muscles. Figure 3 clearly demonstrates the resolution of OCT to delineate bladder morphology needed for bladder cancer diagnosis. To further examine the accuracy of OCT segmentation of bladder morphology, we imaged rat bladder with different layers dissected either mechanically or chemically. Figures 4(A–D) confirms the segmentations of U, LP, and M in full bladder (panel A), although swelling and decreased LP scattering in panel (B) was induced by chemical irritation after removal of U (i.e., protective barrier of the bladder).

To investigate the utility of OCT in the diagnosis and staging of bladder cancers, we performed systemic animal bladder carcinogenesis studies to track the

(A) Full bladder
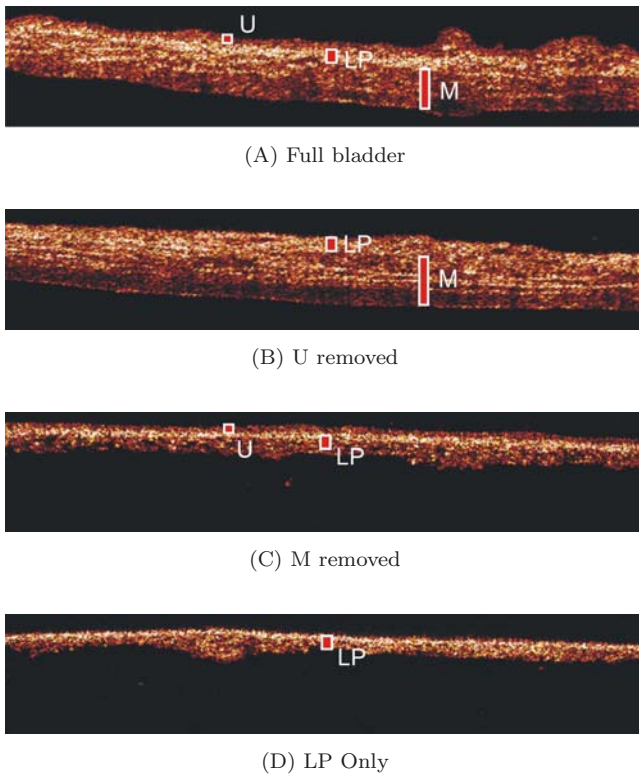

(B) U removed

(C) M removed

(D) LP Only

Fig. 4.   OCT images of rat bladder dissected sequentially to confirm the identifications of bladder layers. (A) Full bladder wall; (B) Urothelium (U) dissected chemically; (C) Muscularis (M) dissected mechanically; (D) Both U and M dissected. Chemical removal of urothelium induced swelling and decreased scattering in the lamina propria (LP).

morphological changes at different stages of tumor growth. Rat bladder cancer models (e.g., by route of MNU or AY27 cell instillations) were employed and OCT imaging was performed identify acute responses (e.g., edema, inflammatory lesions) and the chronic development of dysplasia and TCCs in these rats. Figure 5[25] exemplifies the comparison of the OCT image contrast differences between hyperplasia and TCC. Normal rat bladder has a structural 'template' of a thin low-scattering urothelium (U: $\sim 40\,\mu m$ thick) following high-scattering lamina (LP), muscularis (M), and sometimes the attached fatty layer. Hyperplasia (A) appears as a thick yet low-scattering urothelium U' ($\sim 280\,\mu m$) whereas TCC (b) shows a thick and high-scattering urothelium U'' ($\sim 600\,\mu m$). It was noted that because of their small size, both lesions were difficult to be detected with conventional endoscopy. Quantitative image analysis reveals that compared with normal urothelium, the backscattering ratios are $V_{U'}/V_U \approx 1.11 \pm 0.12$ in the hyperplastic lesion and $V_{U''}/V_U \approx 1.63 \pm 0.17$ in the neoplastic lesion, respectively. In other words, the backscattering ratio $V_{U''}/V_{U'}$ increases roughly 46% from hyperplasia to neoplasia, suggesting the role of backscattering (determined primarily by nuclear-to-cytoplasmic ratio, i.e., NC ratio) as a potential biomarker for OCT diagnosis of early bladder cancer. This diagnostic criterion can be further confirmed by the 3D OCT image as shown in Fig. 6. Compared with 2D, 3D OCT with image animation can provide far more diagnostic details of bladder cancers. The 3D image dataset was captured in $\sim 6\,s$, which was composed of 32 sequential 2D slices with

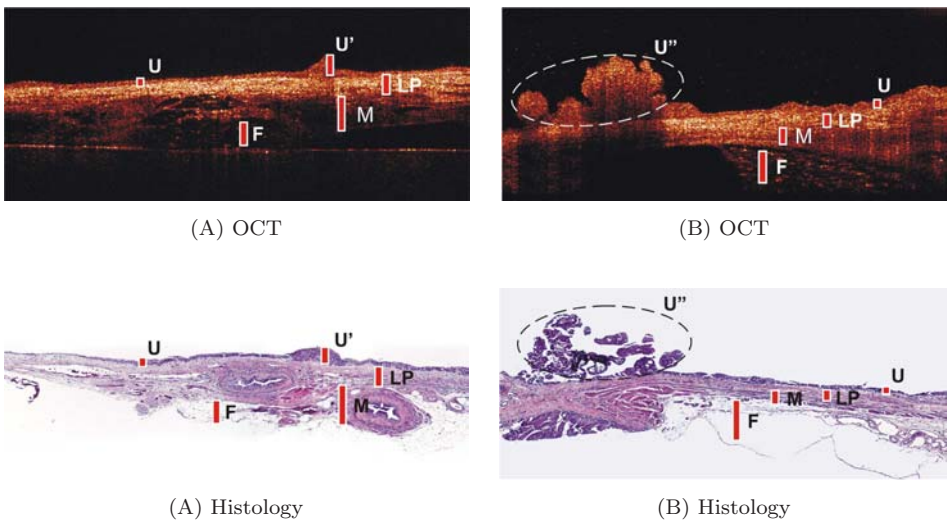
(A) OCT   (B) OCT

(A) Histology   (B) Histology

Fig. 5.   [25] A comparison of hyperplasia (A) and TCC (B) in rat bladders imaged by OCT and histology. U/U'/U'': normal/hyperplastic/neoplastic uroepithelia; LP: lamina propria; M: muscularis, F: fatty layer. Urothelial backscattering ratios are $V_{U'}/V_U \approx 1.11 \pm 0.12$ and $V_{U''}/V_U \approx 1.613 \pm 0.17$, respectively. The TCC in Panel (B) did not invade into LP and M (i.e., stage Ta).
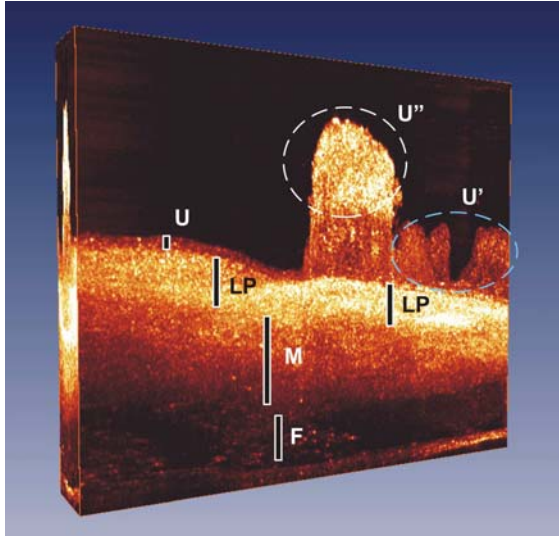
Fig. 6. 3D OCT of a rat bladder *ex vivo*. The image size was L6 mm × D2.1 mm × 2.5 mm, acquired in 6 s. White/blue dashed circles show 1 TCC (U″) and 3 hyperplastic lesions (U′), respectively. U: normal uroepithelium; LP: lamina propria; M: muscularis; F: fatty layer. Urothelial backscattering ratios are $V_{U'}/V_U \approx 1.07$ and $V_{U''}/V_U \approx 1.87$, respectively. U″ is a stage Ta TCC.

80 μm interval. The result clearly indicates that the backscattering in 3 hyperplastic lesions (U′) was low ($V_{U'}/V_U \approx 1.07$) whereas that of the neoplastic lesion (U″) was substantially enhanced ($V_{U''}/V_U \approx 1.87$). Compared with Fig. 5, the 3D OCT image in Fig. 6 drastically enhances the backscattering difference between benign and cancerous lesions.

The results of *ex vivo* human specimen and rat bladder carcinogenesis studies have clearly demonstrated the utility of OCT to delineate bladder morphology at high resolution and to differentiate inflammatory lesions (edema, vasodilatation), urothelial hyperplasia, and TCC, thus justifying the development of COCT for *in vivo* diagnosis of bladder cancers. In vivo porcine OCT cystoscopy was performed first to examine the feasibility of MEMS-based COCT for future *in vivo* clinical diagnosis of bladder cancers. Figure 7 shows an example of simultaneous cystoscopic surface image and cross-sectional COCT image of a normal porcine bladder. Except slightly enlarged speckles due to lower transverse resolution ($\sim 20\,\mu$m) of the early COCT catheter (NA ≈ 0.03), the image quality is comparable to that of *ex vivo* studies such as in Fig. 3. Morphological details of the bladder wall, e.g., U, LP, and M, are clearly delineated based on their backscattering differences.

Based on the promising results of *ex vivo* animal carcinogenesis studies and *in vivo* study, we started clinical study in 2005 to examine the utility and potential limitations of COCT for noninvasive and *in vivo* diagnosis and staging of bladder cancers (TCCs). For all the operating-room (OR) cases that we have performed so
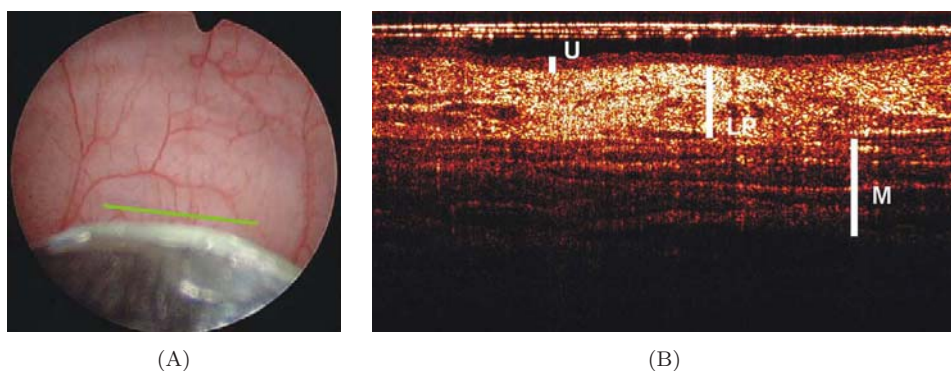
Fig. 7. Results of *in vivo* COCT imaging of normal porcine bladder. (A) surface image; (B) COCT image. U: urothelium, LP: lamina propria, M: muscularis. Green line in (A) indicates the area of simultaneous OCT scan. COCT enables clear delineation of morphological details of porcine bladder (close human homologue) based on their backscattering differences.

far, there is no reported adverse effect, and the COCT imaging procedure was all completed in less than 10 minutes per case. The results presented below are two of the examples from over 130 cases imaged. Figure 8[39] shows the surface, COCT, and the corresponding histological images of a typical normal human bladder *in vivo*. As expected, the OCT image closely resembles those in Fig. 3 (human bladder specimen *ex vivo*) and Fig. 7 (porcine bladder *in vivo*), the morphological characteristics, e.g., low scattering thin urothelium (U), high-scattering heterogeneous lamina propria (LP), and the slightly lower scattering muscularis (M) correlate well with the corresponding H&E histological evaluation. Figure 9[39] shows a typical human TCC. The results indicate that although surface imaging can roughly give the cancer boundary, COCT — due to depth resolution — can see through the large papillary TCC to precisely mark the lateral cancer margin with surrounding normal bladder as highlighted by the yellow dash line. Here, TCC diagnosis was based on increased urothelial backscattering heterogeneity (e.g., papillary features, dark holes) as a result of random, excessive nature of carcinogenesis. It is noted that because of decrease in imaging depth within the cancerous lesion, COCT staging of bladder tumors is limited to Ta and T1 without substantive outgrowth. The results of our clinical study reveal that owing to the high resolution, dynamic range and large FOV, our MEMS-based COCT can diagnose bladder cancers, differentiate cancer residuals from resection-induced scars, and to precisely guide tumor resections.

4. Potential Problems and Future Study

Results based on *in vivo* clinical imaging diagnosis demonstrate the ability of our MEMS-based COCT to delineate bladder layers at high resolution (e.g., Fig. 8) and the potential to drastically enhance the diagnosis of bladder cancers (e.g., Fig. 9). As a blind study, COCT diagnosis was compared with the corresponding histological
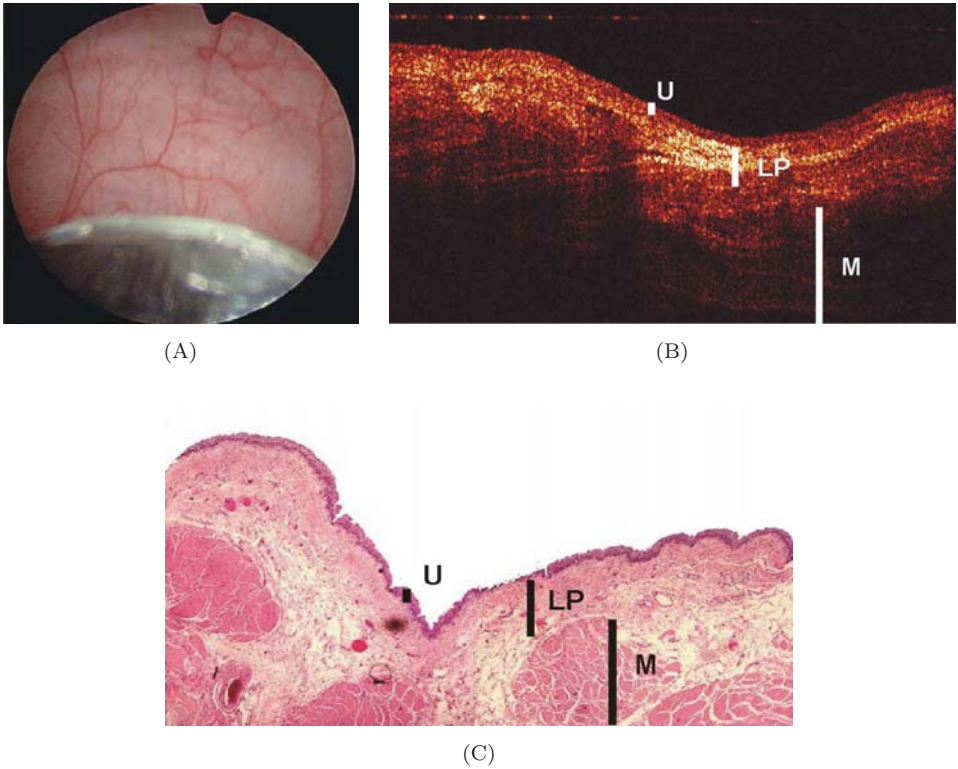
(A)   (B)

(C)

Fig. 8.   [39]Results of *in vivo* COCT imaging of normal human bladder. (A) surface image; (B) COCT image; (C) Histology. U: urothelium, LP: lamina propria, M: muscularis. Image sizes: $\phi 12\,\mathrm{mm}$ for (A) and $2.1 \times 4.7\,\mathrm{mm}^2$ for (B) and (C).

evaluations from the specimens either biopsied or resected (i.e., TURBT) as the gold standard for clinical diagnosis. It was found that COCT images correlated well with histology. For instance, the *in vivo* COCT measurement of the urothelial thickness of $d_U = 67.9 \pm 5.6\,\mu\mathrm{m}$ matched the histological evaluation of $d_U = 62.8 \pm 4.1\,\mu\mathrm{m}$, appearing as a homogeneous, low-scattering thin layer, as shown in Fig. 8. Clinical statistics indicate that the overall diagnostic sensitivity is $\sim 92\%$. The diagnostic specificity is $\sim 85\%$ and continues to improve with the increase of the enrolled cases. In addition to enhancing the diagnosis of flat TCCs such as CIS, COCT has the great potential to enhance the diagnosis of tumor residuals post TURBT, which remains a clinical challenge because both types of lesions show rugged surface appearance and are therefore difficult to differentiate. However, COCT can effectively differentiate them based on their backscattering difference and embedded local urothelial heterogeneity. Results also demonstrate the resolution of COCT to accurately locate the cancer margins in the lateral directions.

Some discrepancies and potential problems have been observed during the clinical diagnoses of bladder cancers. For instance, results of rat bladder carcinogenesis
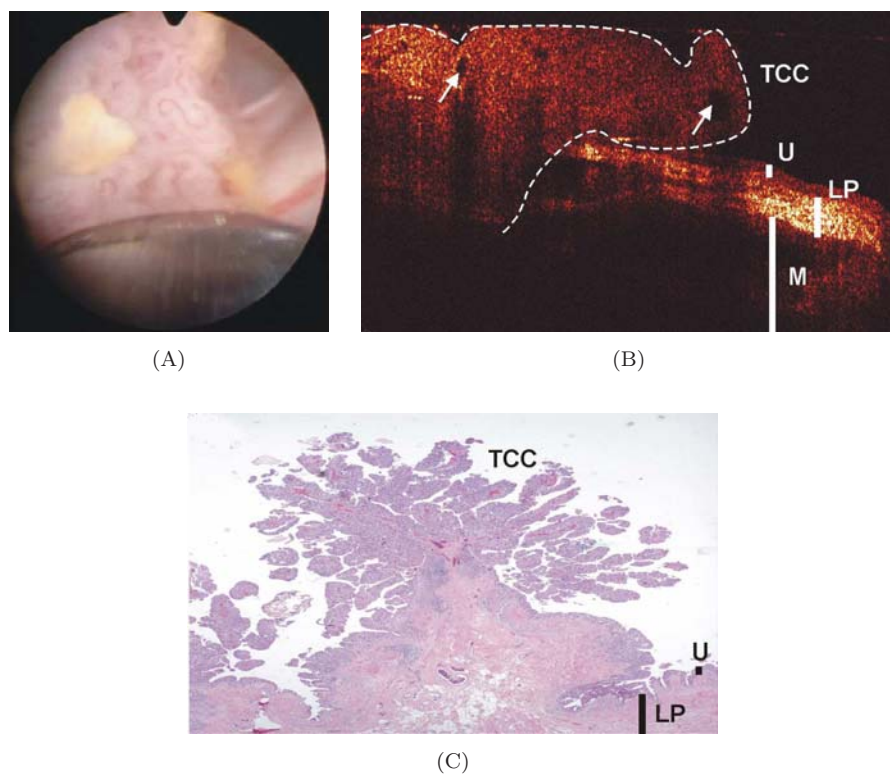
(A)

(B)

(C)

Fig. 9.   [39]Results of *in vivo* COCT imaging of TCC (low grade 1/3, stage T1) in human blad-
der. (A) surface image; (B) COCT image; (C) Histology. U: urothelium, LP: lamina propria, M:
muscularis. Image sizes: $\phi 12$ mm for (A) and 2.1×4.5 mm^2 for (B) and (C). Papillary TCC was
identified by enhanced heterogeneity (e.g., honey nests) as pointed by arrows.

studies have revealed enhanced urothelial backscattering in cancerous lesions
(Figs. 5 and 6); however, our clinical studies indicate that the majority of human
TCCs ($> 75\%$) show no obvious increase in urothelial backscattering. Based on
the facts, we modified our diagnostic criteria as imaging the transition between the
lesion (e.g., TCC, CIS) and the normal bladder region and the detection of enhanced
urothelial heterogeneity as a biomarker in terms of the excessive growing nature of
carcinogenesis. Clinical results seem to well support the effectiveness of the current
diagnostic results, showing promising correlation with histological evaluation. The
low false positives were mostly from early cases based on previous diagnostic criteria
of backscattering enhancement and few cases of flat low-grade TCCs. Fortunately,
unlike animal carcinogenesis studies, urothelial hyperplasia is uncommon in clinical
cases, because this type of lesions exhibit thickened low backscattering and thus can
induce difficulties for OCT to differentiate them from low-grade early TCCs, which
requires subcellular imaging for cell-type differentiation. To futher address these
issues, we have recently invented subcellular OCT imaging based on time-lapse

ultrahigh-resolution OCT (TL-uOCT) taking advantage of micro motions in living cells to effectively reduce speckle noise and thus to uncover subcellular details.[40] Unlike optical coherence microscopy that achieves subcellular imaging by confocality, TL-uOCT has over drastically increased depth of field due to lower NA tolerance (e.g., NA = 0.25) that allows subcellular imaging of urothelium (at focus) and high-resolution imaging into lamina propria and potentially upper muscularis over $700\,\mu m$ without focal tracking, thus highly suitable for in vivo imaging. We are in the development of endoscopic TL-uOCT for future more accurate diagnosis and potentially grading of CIS and other flat early TCCs. Although current COCT can detect most of the CIS, it fails grade them, which is critical for the effective treatment of CIS.

A potential drawback is the capability of COCT for staging bladder cancers. Our studies reveal that due to reduced imaging depth in TCCs as a result of increased local heterogeneity and vasodilatations, COCT may has limited applications for staging the invasion of large, outgrowing TCCs (e.g., T1 or higher). This poses the potential limitation in providing cancer margins in the depth direction to guide tumor resections (TURBT). As this could be the physical limitations to the OCT technology we have recently tackled the challenge by combining OCT with ultrasound imaging (HFUS).[41] Our preliminary results based on animal carcinogenesis study demonstrate the great potential for combing these two techniques which may compliment each other: the high-resolution of OCT can enhance the diagnosis of TCC which HFUS often fails whereas HFUS can stage the invasion of TCC to stage T2 or even higher that OCT fails due to limited imaging depth.

Another promising approach is to implement simultaneous SDOCT and Doppler SDOCT to enhance the diagnosis. Our preliminary results suggest that Doppler COCT can detect fibro vascular cords in TCC lesions and thus provides more accurate diagnosis. However, it has been noticed that that accurate endoscopic flow measurement is hindered by several problems, including artifacts induced by angle distribution of bladder vessels, motion induced artifacts and of phase noises, local blood flow occlusion during *in vivo* COCT imaging. Studies are still under way to provide better solutions.

In conclusion, recent technological advances in OCT, in particular endoscopic OCT, have drastically elevated the capabilities of OCT for *in vivo* diagnostic applications in various clinical arenas. As an enabling imaging modality, COCT has demonstrated its unique potential in enhancing the current endoscopic procedures in the diagnosis of early bladder cancers. Results of *ex vivo* animal carcinogenesis studies demonstrate the resolution of OCT for delineating the morphological details of bladder wall and for high-resolution imaging diagnosis of bladder cancers. Further *in vivo* clinical study demonstrates that MEMS-based COCT is suitable for clinical uses to drastically enhance the current procedures in the diagnosis of early bladder cancers.

References

1. American Cancer Society, *Cancer Facts & Figures 2007.* http://www.cancer.org/downloads/STT/CAFF2007PWSecured.pdf, 2007.
2. M. Kriegmair *et al.*, Detection of early bladder cancer by 5-aminolevulinic acid induced porphyrin fluorescence, *Journal of Urology* **155**(1), 105–109 (1996).
3. D. Zaak *et al.*, Quantification of 5-aminolevulinic acid induced fluorescence improves the specificity of bladder cancer detection, *Journal of Urology* **166**(5), 1665–1668 (2001).
4. D. Huang *et al.*, Optical Coherence Tomography, *Science* **254**(5035), 1178–1181 (1991).
5. R. A. Leitgeb *et al.*, Real-time measurement of in vitro flow by Fourier-domain color Doppler optical coherence tomography, *Optics Letters* **29**(2), 171–173 (2004).
6. B. J. Vakoc *et al.*, Phase-resolved optical frequency domain imaging, *Optics Express*, **13**(14), 5483–5493 (2005).
7. M. Wojtkowski *et al.*, Three-dimensional retinal imaging with high-speed ultrahigh-resolution optical coherence tomography, *Ophthalmology*, **112**(10), 1734–1746 (2005).
8. Z. P. Chen *et al.*, Optical Doppler tomography, *Ieee Journal of Selected Topics in Quantum Electronics* **5**(4), 1134–1142 (1999).
9. S. Yazdanfar, M. D. Kulkarni and J. A. Izatt, High resolution imaging of in vivo cardiac dynamics using color Doppler optical coherence tomography, *Optics Express* **1**(13), 424–431 (1997).
10. J. F. de Boer *et al.*, Imaging thermally damaged tissue by polarization sensitive optical coherence tomography, *Optics Express* **3**(6), 212–218 (1998).
11. U. Morgner *et al.*, Spectroscopic optical coherence tomography, *Optics Letters* **25**(2), 111–113 (2000).
12. X. D. Wang and L. H. V. Wang, Propagation of polarized light in birefringent turbid media: A Monte Carlo study, *Journal of Biomedical Optics* **7**(3), 279–290 (2002).
13. B. Bouma *et al.*, High-resolution optical coherence tomographic imaging using a mode-locked Ti-Al2o3 laser source, *Optics Letters* **20**(13) (1995) 1486–1488.
14. S. A. Boppart *et al.*, In vivo cellular optical coherence tomography imaging, *Nature Medicine* **4**(7), 861–865 (1998).
15. W. Drexler, Ultrahigh-resolution optical coherence tomography, *Journal of Biomedical Optics* **9**(1), 47–74 (2004).
16. S. Tang *et al.*, Imaging subcellular scattering contrast by using combined optical coherence and multiphoton microscopy, *Optics Letters* **32**(5), 503–505 (2007).
17. G. J. Tearney *et al.*, In vivo endoscopic optical biopsy with optical coherence tomography, *Science* **276**(5321), 2037–2039, (1997).
18. Y.-T. Pan and D. L. Farkas, Dual-color, 3-D imaging of biological tissues using optical coherence tomography, *Journal of Biomedical Optics* **3**(4), 446–455 (1998).
19. F. I. Feldchtein *et al.*, In vivo OCT imaging of hard and soft tissue of the oral cavity, *Optics Express* **3**(6), 239–250 (1998).
20. J. A. Izatt *et al.*, Optical coherence tomography and microscopy in gastrointestinal tissues. *Ieee Journal of Selected Topics in Quantum Electronics* **2**(4), 1017–1028, (1996).
21. A. M. Sergeev *et al.*, In vivo endoscopic OCT imaging of precancer and cancer states of human mucosa, *Optics Express* **1**(13), 432–440 (1997).
22. N. Mikhail-Hanna *et al.*, Optical coherence tomography of the lung and lower airway, *Chest* **124**(4), 77s–77s, (2003).

23. E. V. Zagaynova *et al.*, In vivo optical coherence tomography feasibility for bladder disease, *Journal of Urology* **167**(3), 1492–1496 (2002).

24. Y. T. Pan *et al.*, Detection of tumorigenesis in rat bladders with optical coherence tomography, *Medical Physics*, **28**(12), 2432–2440 (2001).

25. T. Q. Xie, M. L. Zeidel and Y. T. Pan, Detection of tumorigenesis in urinary bladder with optical coherence tomography: optical characterization of morphological changes, *Optics Express* **10**(24), 1431–1443 (2002).

26. P. F. Escobar *et al.*, Diagnostic efficacy of optical coherence tomography in the management of preinvasive and invasive cancer of uterine cervix and vulva, *International Journal of Gynecological Cancer* **14**(3), 470–474 (2004).

27. M. E. Brezinski *et al.*, Assessing atherosclerotic plaque morphology: Comparison of optical coherence tomography and high frequency intravascular ultrasound, *Heart* **77**(5), 397–403 (1997).

28. B. E. Bouma and G. J. Tearney, *Handbook of Optical Coherence Tomography* (Marcel Dekker, Inc., 2002).

29. G. Hausler and W. M. Lindner, "Coherence Radar" and "Spectral Radar"–New Tools for Dermatological Diagnosis, *Journal Of Biomedical Optics* **3**(1), 21–31 (1998).

30. G. J. Tearney, B. E. Bouma and J. G. Fujimoto, High-speed phase- and group-delay scanning with a grating-based phase control delay line, *Optics Letters* **22**(23), 1811 (1997).

31. T. Q. Xie, Z. G. Wang and Y. T. Pan, High-speed optical coherence tomography using fiberoptic acousto-optic phase modulation, *Optics Express*, **11**(24), 3210 (2003).

32. W. Jung *et al.*, Three-dimensional endoscopic optical coherence tomography by use of a two-axis microelectromechanical scanning mirror, *Applied Physics Letters*, **88**(16) (2006).

33. Y. T. Pan, H. K. Xie and G. K. Fedder, Endoscopic optical coherence tomography based on a microelectromechanical mirror, *Optics Letters* **26**(24), 1966–1968 (2001).

34. H. Toshiyoshi *et al.*, Linearization of electrostatically actuated surface micromachined 2-D optical scanner, *Journal of Microelectromechanical Systems* **10**(2), 205–214 (2001).

35. A. D. Aguirre *et al.*, Two-axis MEMS scanning catheter for ultrahigh resolution three-dimensional and en face imaging, *Optics Express* **15**(5), 2445–2453, (2007).

36. T. Q. Xie *et al.*, Endoscopic optical coherence tomography with new MEMS mirror, *Electronics Letters* **39**(21), 1535–1536 (2003).

37. Y. T. Pan *et al.*, Enhancing early bladder cancer detection with fluorescence-guided endoscopic optical coherence tomography, *Optics Letters* **28**(24), 2485–2487, (2003).

38. Z. G. Wang *et al.*, Fluorescence guided optical coherence tomography for the diagnosis of early bladder cancer in a rat model, *Journal of Urology* **174**(6), 2376–2381 (2005).

39. Z. G. Wang *et al.*, In vivo bladder imaging with microelectromechanical systems-based endoscopic spectral domain optical coherence tomography, *Journal of Biomedical Optics* **12**(3), (2007).

40. Y. T. Pan *et al.*, Subcellular imaging of epithelium with time-lapse optical coherence tomography, *Journal of Biomedical Optics* **12**(5) (2007).

41. Z. Yuan, Z. Wang and Y. Pan, High-resolution imaging diagnosis and staging of bladder cancer: A comparison between optical coherence tomography and high-frequency ultrasound. *Journal of Biomedical Optics*, accepted, (2008).